AIAA-94-2851

Segmented Ion Engine Operation and Performance

John R. Brophy*, Juergen Mueller,** Lewis C. Pless, ***
Mike Tierney,† Keith D. Goodfellow**, and John R. Anderson**
Jet Propulsion Laboratory
California Institute of Technology
Pasadena, California

The continuing trend toward smaller and smaller planetary spacecraft to enable the use of smaller, less expensive launch vehicles has motivated an examination of new approaches to reduce the sire. and mass of xenon ion propulsion systems for these new spacecraft. A system is proposed which is based on the use of a single 4x15-cm segmented ion thruster operated from a single internally redundant power processing unit. An engine input power throttling range of *380* to 4640 W is projected. The design and operation over a power range of 600 to 2400 W of a laboratory model segmented ion engine equipped with carbon-carbon grids is presented. There appear to be no problems associated with interactions with multiple ion sources operating from a single set of high voltage power supplies, neutralization of multiple ion sources from a single centrally-located neutralizer, or operation of flat, thin carbon-carbon grids.

Introduction

In the ongoing efforts to reduce the cost of solar system exploration missions, projections of future spacecraft sizes and masses continue to&crease in order to enable the usc of smaller, less expensive launch vehicles. High specific impulse ion propulsion systems can potentially provide substantial mass and volume reductions for high energy missions (such as small body rendezvous missions, sample return missions, and outer planet flybys]). However, as the mass and size of potential host spacecraft decreases, the dry mass and volume of the ion propulsion system must also decrease. This is generally accomplished in system studies by reducing the power level of the propulsion system to obtain a corresponding reduction in the number of engines and associated hardware (i.e., power conditioning units, propellant feed system components, gimbals, cabling and support structure). Even with these reductions current projections for the mass of primary ion propulsion systems indicate that the dry mass is comparable to the propellant mass for planetary missions of near-term interest.[2] For Earth orbital missions such as north-south stationkeeping, the dry mass fraction can also bc large. The flight ion propulsion system for ETS-VI has a dry mass that is approximately twice the propellant mass required for the 10 year mission.[3] Never-the-less, even with these large dry mass fractions, ion propulsion bawd systems still show a substantial benefit relative to other kinds of propulsion systems. The relatively large ion propulsion system dry mass fraction suggests that there is room for considerable improvements, especially for small spacecraft.

To achieve further reductions in dry mass requires the examination of different system architectures and the usc of advanced technologies. The segmented ion enginc[4,5] described herein consists of four 15-cm diameter ion sources integrated structurally and electrically into a single compact, lightweight unit. The ion sources are equipped with carbon-carbon grids in a 3-grid SAND[6] configuration to increase the electrodc life and the projected propulsion system total impulse capability.

* Supervisor, Advanced Propulsion Technology Group, Member AIAA
**Member of the Technical Staff, Advanced Propulsion Technology Group, Member AIAA
** *Member of the Technical Staff, Electric power Systems Section
'Graduate Student, California Institute of Technology

For very small planetary spacecraft, i.e., those with an injected wet mass of approximately 500 kg, it is proposed that a light weight propulsion system could be based on the usc of a single segmented ion engine and a single internally redundant power conditioning unit, Projections of the dry mass of such a system, along with the corresponding performance in terms of input power requirements, thrust, specific impulse and total impulse capabilities will be presented. In addition, the design and preliminary tests of a 4x15-cm segmented ion engine with carbon-carbon grids is presented.

The expected advantages' of using a single 4x15-cm segmented ion engine as the basis for a small spacecraft primary propulsion system are:

1. The existence of multiple ion sources in the segmented engine provide built in redundancy for operation at throttled conditions where some of the ion sources do not need to be operated.
2. Accomplishing major power throttling by shutting off individual ion sources enables the remaining sources to operate closer to their maximum power, maximum efficiency point.
3. Ion sources in the segmented engine that are shut down as a result of throttled operation are no longer subject to wear and maybe used later in the mission.
4. Structural integration of the ion sources into the segmented configuration results in a lower mass system than the use of multiple separate small ion engines.
5. The relatively small diameter of the ion sources in the 4x1 5-cm segmented engine facilitate the implementation of advanced grid technologies such as the usc of carbon-carbon grids.

Thruster Design

The 4x1 5-cm segmented ion thruster shown in Fig, 1 is made up of fbur 15-cm diameter ion sources of the type described in Ref. 4. Each ion source is a modified, scaled-down version of the NASA light-weight, 30-cm diameter ring-cusp thruster.[7] Each discharge chamber body is made of 6061 aluminum and the ring-cusp magnetic field configuration is formed from two rings of samarium-cobalt magnets; one positioned at the upstream end near the cathode and the other at the downstream end near the accelerator system. Two of the ion sources have the polarity of their magnet rings reversed to give a right- and left-handedness to the sources, In the segmented engine configuration, the ion sources (or segments) arc integrated such that segments A and C are right-handed and B and D arc left-handed.

The ion source segments are integrated onto a base plate structure at ground potential. Electrical insulators between the segments and to the centrally located neutralizer assembly are used to make the overall structure very rigid Each ion source is electrically isolated from the others. Electrical integration of the ion source segments is accomplished at the power supplies. This enables a faulty ion source to be isolated from the others. A single, Centrally-located neutralizer cathode i.. used to neutralize all of the ion sources, For a propulsion system which consists of a single segmented ion engine, a second neutralizer cathode would likely be included for redundancy.

A light-weight, compact, low-pressure propellant isolator (designated the Thogalator-III) was developed to isolate the high voltage ion sources from the grounded propellant feed system. Two Thogalator-III isolators are used for each ion source (one each for the main and cathode xenon flows). This isolator design, has a mass of approximately 33 g and a measured leakage current of less than 3 μA at 7.5 kV in bell-jar tests at the low-pressure xenon flow rates required for operation of the segmented ion engine.

Grids

Three-sets of 3-grid ion accelerator systems were fabricated from carbon-carbon. A fourth set was damaged during fabrication and couldn't be used. Ion source segments A, B, and C were equipped with the carbon-carbon grids. Segment D was equipped with a 3-grid, graphite accelerator system as described in Ref. 4, The geometries of the carbon-carbon and graphite grids are summarized in Table. 1. Details of the fabrication and operation of the carbon-carbon grids arc given in Ref. 8,

Apparatus and Procedure

Segmented engine tests were conducted in a 2.4-m diameter by 5-m stainless steel vacuum chamber. Three large oil diffusion pumps provide an effective pumping speed on xenon of 14,000 L/s. The beam target and cylindrical side walls of the vacuum chamber are lined in

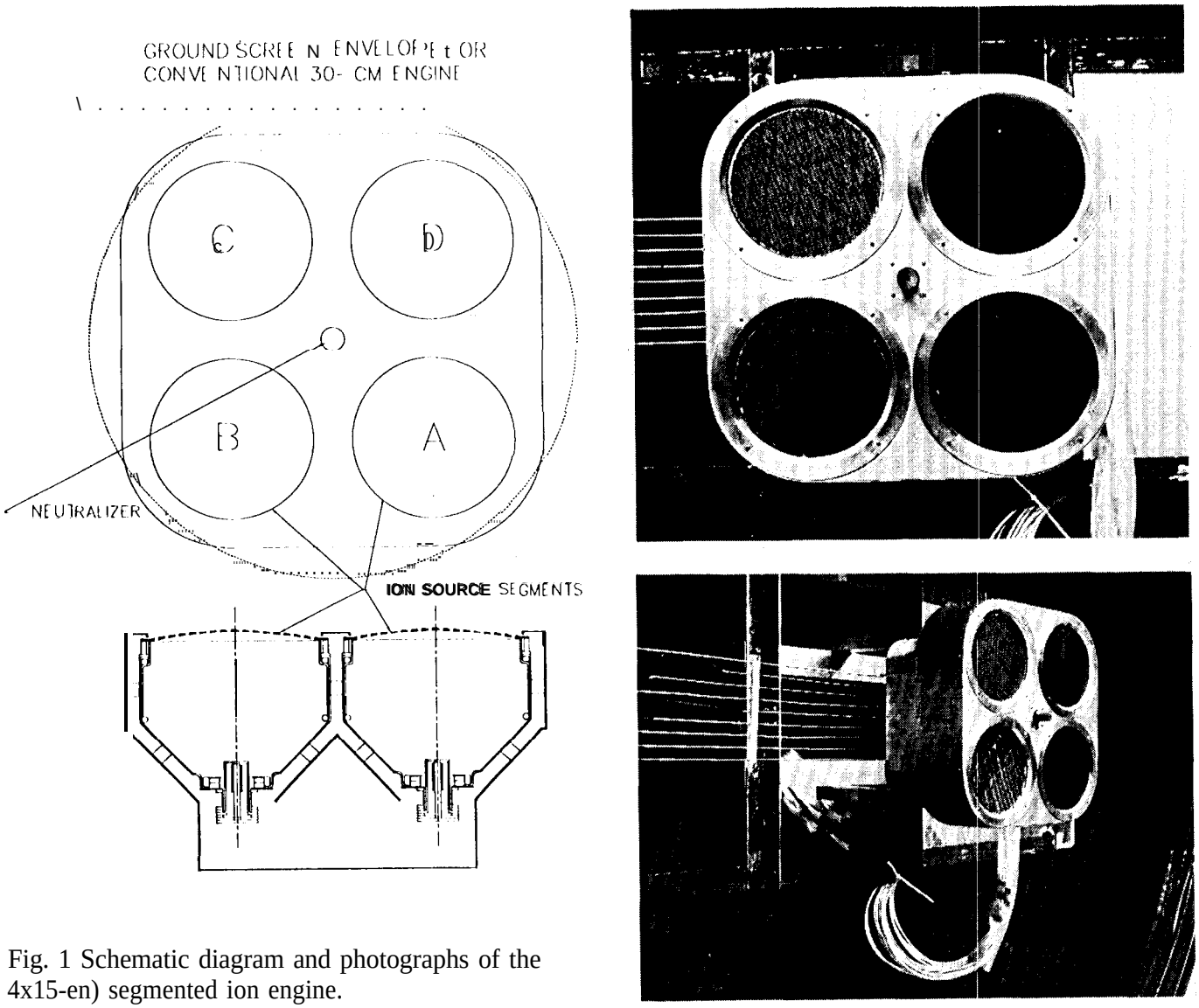

Fig. 1 Schematic diagram and photographs of the 4x15-en) segmented ion engine.

graphite to minimize the rate of material back-sputtered to the engine during testing.

Power Supplies

The power supply block diagram for the segmented ion engine is given in Fig. 2. A single set of high voltage power supplies (screen, accelerator and decclerator) is used and each ion source segment has a dedicated discharge supply. With multiple segments operating, an arc occurring on any one of the operating segments will cause all of them to experience a high voltage recycle (since there is only onc set of 'high voltage power supplies). The high voltage recycle algorithm includes scaling back the discharge current to all operating segments before the high voltage is reestablished. The discharge currents in each segment are then brought back up to their normal run levels. The discharge supply for each ion source segment also used to heat the cathode during the start-up procedure. Separate start-up power supplies for each segment (not shown in Fig. 2) are attached to the keeper/starter electrodes and are used to start the cathodes. These supplies arc probably not necessary since the cathodes could always be started with less than 32 volts applied to thc starter electrode. Future tests will be performed to see if the discharge power supplies ean be used to start the cathodes.

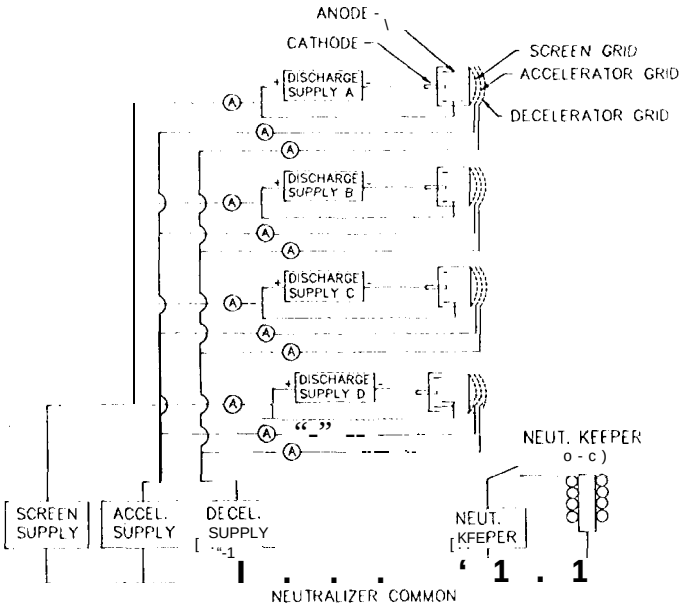

Fig. 2 Power Supply Block Diagram for the segmented ion engine.

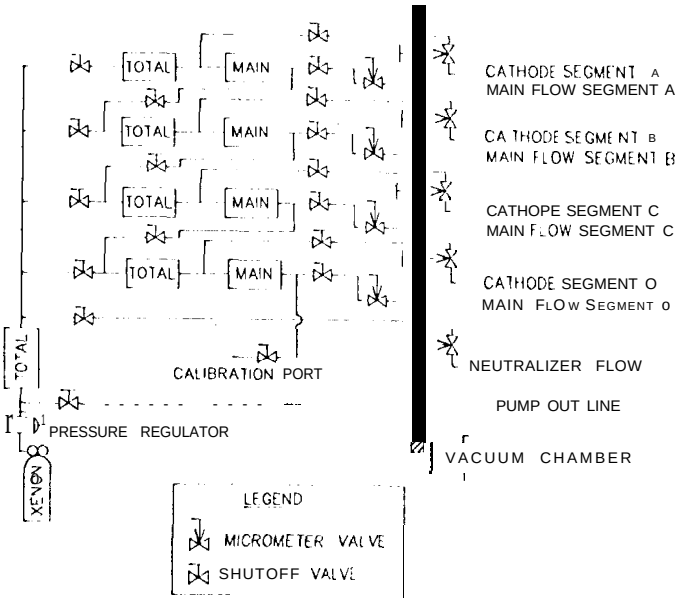

Fig. 3 Flow system schematic for the segmented ion engine.

Laboratory power supplies arc used throughout, For the main discharge, switching power supplies from Power 10 that are O-50 V and 20 A arc used The high voltage screen supply is a custom 12 kW (6 A and 2 kV) supply made by Spellman. The cathode start supplies and neutralizer cathode start and run supplies arc feroresonant supplies made by Kepco.

Propellant Feed System

A schematic of the propellant feed system is shown in Fig. 3. This system provides independent control of the cathode and main flow for each segment and for the neutralizer cathode. The propellant flow meters (Tylan model FM-380) are configured to measure the main and total flow for each segment, Cathode flow rates are determined by subtracting the measured main flow from the measured total flow. A ninth flow meter is used to measure the total flow rate into the segmented ion engine including the neutralizer. The neutralizer flow rate is determined by subtracting the sum of the total flows for the operating segments from the measured total flow for the Whole engine.

By opening and closing the proper valves, the flow system can be configured to enable the calibration of all of the flow meters, simultaneously and in situ. The flow meters were calibrated in this fashion on xenon using a Hastings model HBM-1A, soap bubble type calibration kit. Micrometer valves were used to control the main and cathode flow rates for each segment, The cathode flow micrometer valves were positioned inside the vacuum system so that the xenon supply pressure was above atmospheric pressure at the vacuum feed through. This guarantees that no air can leak into the cathode feed lines. Mechanical rotary feed through were used to manipulate the cathode micrometer valves from outside the vacuum system.

Beam Probe System

A Faraday probe rack was attached to a 3-axis, computer controlled positioning system in order to measure the ion beam current density profiles as a function of position downstream from the engine with different combinations of segments operating, The probe system is described in detail in Ref. 9.

Results

Preliminary performance data has been obtained for the segmented engine. These data were obtained over a relatively short amount of testing and the full operating envelope of the engine has not yet been explored.

Discharge Chamber Performance

Three of the four ion source segments (A, B and C) in the segmented ion engine were equipped with carbon-carbon grids. Segment D was equipped with dished graphite grids which could not be gapped properly due to what appeared to be slight differences in the curvatures of the electrodes. Therefore, performance characteristics are given only for the three segments with the carbon-carbon grids.

Comparison of discharge chamber performance curves for segments A and C is given in Fig. 4. The propellant efficiencies in this and all discharge chamber performance curves in this paper have been corrected for neutral atom backflow from the facility, but not for the presence of multiply charged ions. The backflow correction was performed assuming a xenon atom temperature in the vacuum chamber of 300K and that the restriction to xenon flow back into the engine was determined solely by the open area fraction of the accelerator grid. No attempt was made to account for the finite thickness of the accelerator grid or for the existence of the decelerator and screen grids, thus making the correction somewhat conservative. The numbers adjacent to the data symbols indicate the corresponding discharge voltage, The total discharge chamber propellant flow rate for segment A was 0.60 mg/s and for segment B is was 0.64 mg/s for the data in Fig. 4. The performance of these two segments appears to be reasonably similar.

The performance of segments B and C are compared in Fig. 5 for a total discharge chamber propellant flow rate of 0.64 mg/s. These agree relatively well with those in Fig, 4. The indicated beam ion production energy for segment C in Fig, 5 is less than for segment B because the accelerator grid impingement current was higher for segment B than for C at the same extracted beam current. Consequentl y, segment B must produce slightly more ions than C to extract the same beam current resulting in a slightly higher beam ion production energy. This effect is swamped by the difference in discharge voltages at the higher propellant efficiencies..

The performance of segment C is given in Fig. 6 for total discharge chamber propellant flow rates of 0.73 and 1.01 mg/s. 'The beam ion production energy is slightly lower for operation at the higher total flow rates as would be expected. The 15-cm diameter ring-cusp discharge chambers used in the segmented ion engine appear to give relatively consistent, reasonably good performance

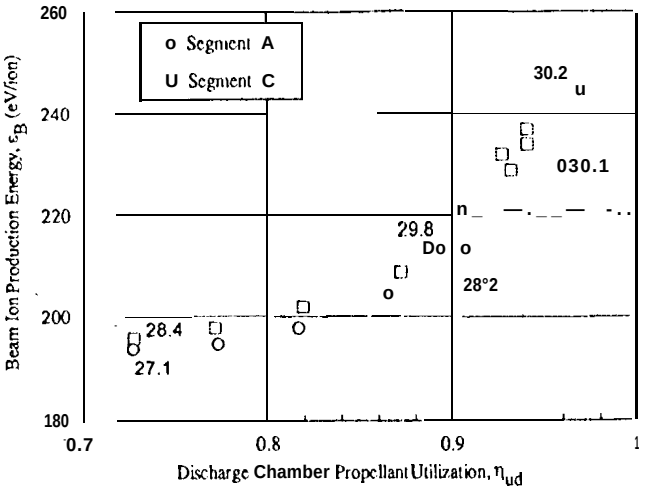

Fig. 4 Comparison of segment A and C discharge chamber performance (screen, accelerator and decelerator voltages of 1200, -100 and -100 V, respectively).

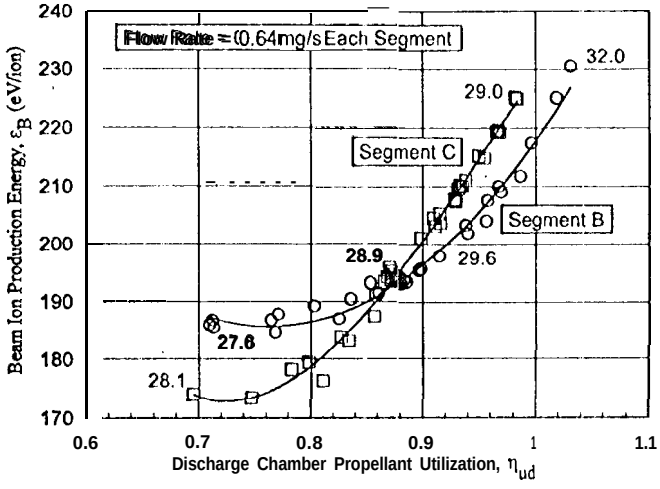

Fig. 5 Comparison of segment B and C discharge chamber performance (screen, accelerator and decelerator voltages of 1300, -150 and -100 V, respectively.

Sensitivity to Cathode and Main Flow Rate Variation..

The effect of cathode flow rate variations on the discharge voltage and beam current are given in Fig. 7 for segments A and C. The straight life curve tits in these graphs are for the segment A data only, but appear to bc consistent with the segment C data which was collected over a smaller flow rate variation range. The sensitivities of the discharge voltage and beam current of -6.9 V/seem

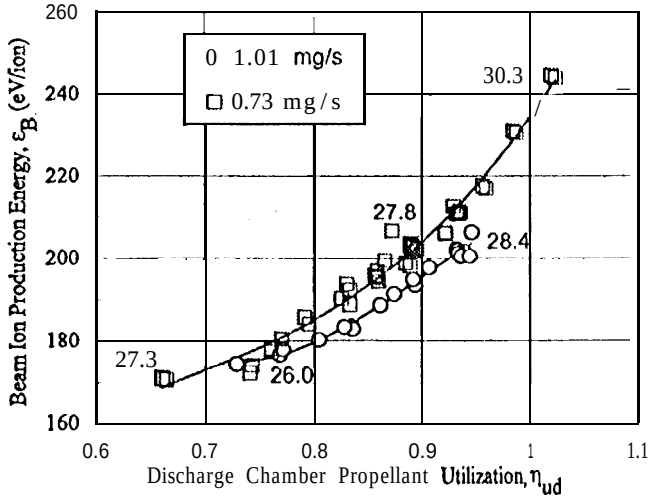

Fig. 6 Segment C discharge, chamber performance at two mass flow rates (screen, accelerator and decelerator voltages of 1320, -100, and -75 V, respectively).

(0.36 %/%) and -0.11 A/sccm (-0.38 %/%) to cathode flow rate variations appear to be comparable to those of other ring-cusp thrusters.[7,10]

The effect of main flow rate variations on the discharge voltage and beam current for segment A are given in Fig. 8. These data indicate that for main flow rate variations of less than 4 % there is essentially no change in the discharge voltage or beam current. The effect of larger main flow rate variations is given in Fig. 9 for segment C. Even for these larger main flow rate variations (up to 25 %), the discharge voltage and beam current sensitivities of -0.43 V/seem (-0.08 %/%) and 4.5 mA/seem (0.06 %/%) remain small,

Carbon-Carbon Grid Operation

The performance of the carbon-carbon grids was measured for each of the three accelerator systems on segments A, B and C. An example of the perveance is given in Fig. 10 for segment C. The perveance is poorer than that obtained with the 3-grid molybdenum accelerator system described in Ref. 4 where an impingement limited total voltage of 1000 V was obtained for a beam current of 500 mA. This is almost certainly due to the very thick accelerator grid used with the carbon-carbon grids. The accelerator grid is 940 , pm thick compared to the molybdenum grid thickness of 360 µm. To improve the

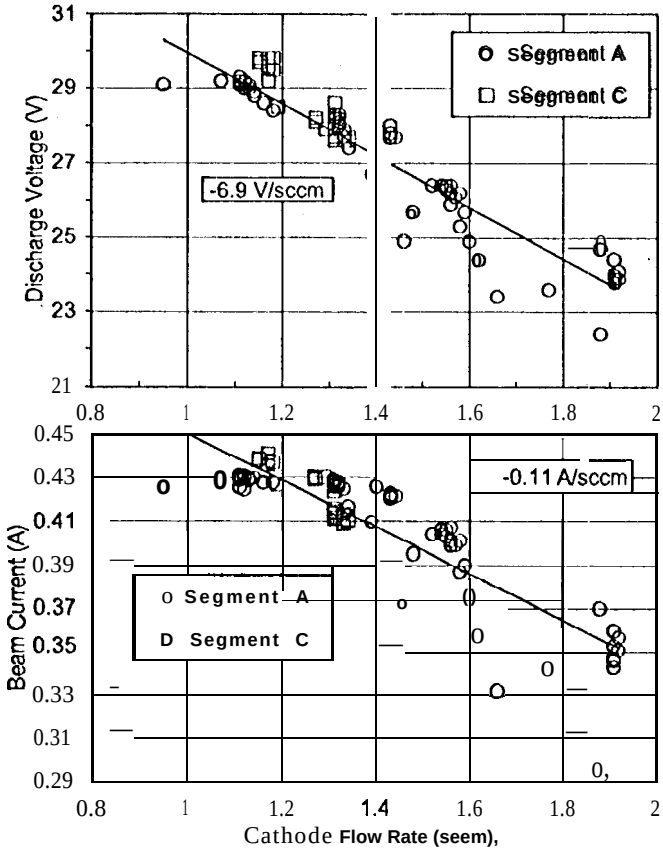

Fig. 7 Effect of cathode flow rate variations (screen, accelerator and decelerator voltages of 1296,.-107 and 076 V, respectively, main flow rate of 5.1 seem).

perveance capabilities of the carbon-carbon grids, the accelerator and decelerator electrodes will be lapped down to a thickness of approximately 500 µm. This can be done while still maintaining the symmetry of the carbon fiber lay-up.[8]

The three-grid accelerator systems were operated in the SAND[6] configuration which includes a small negative bias (-50 to -100 V) on the decelerator grid. The very thick accelerator grids used in these accelerator systems enabled operation at very high net-to-total voltage ratios (R) even without the negative accelerator grid bias. However, the highest R-ratio achieved (0.96) was still obtained with a negative decelerator grid bias. Operation with a beam current of 500 mA on each of the three segments with carbon-carbon grids was easily achieved with an accelerator grid voltage of only -100 V. Although the sputter yield of carbon-carbon at ion energies of a few

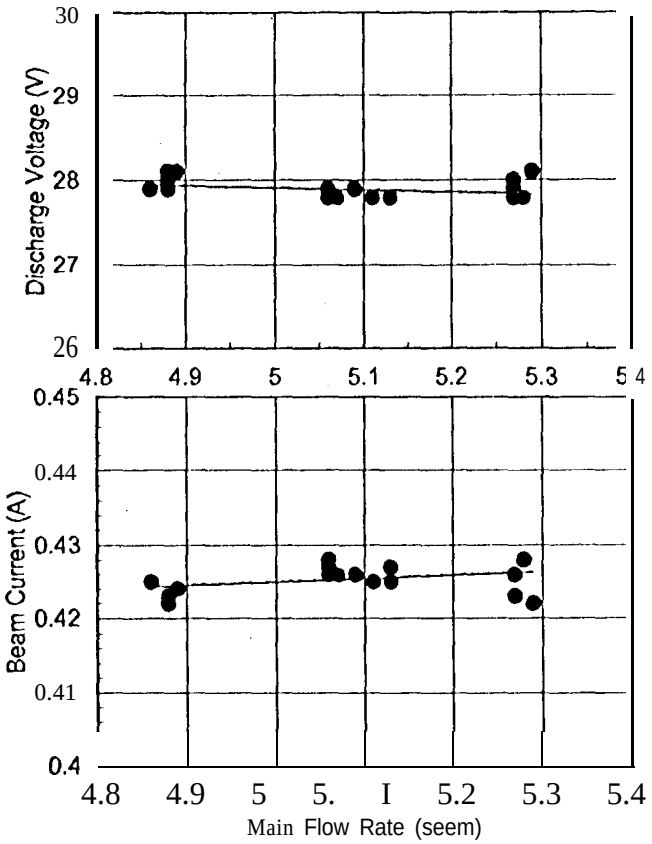

Fig. 8 Effect of small main flow rate changes (screen, accelerator, and decelerator grid voltages of 1296, -107, and -76 V, respectively, cathode flow rate of 1.39 seem).

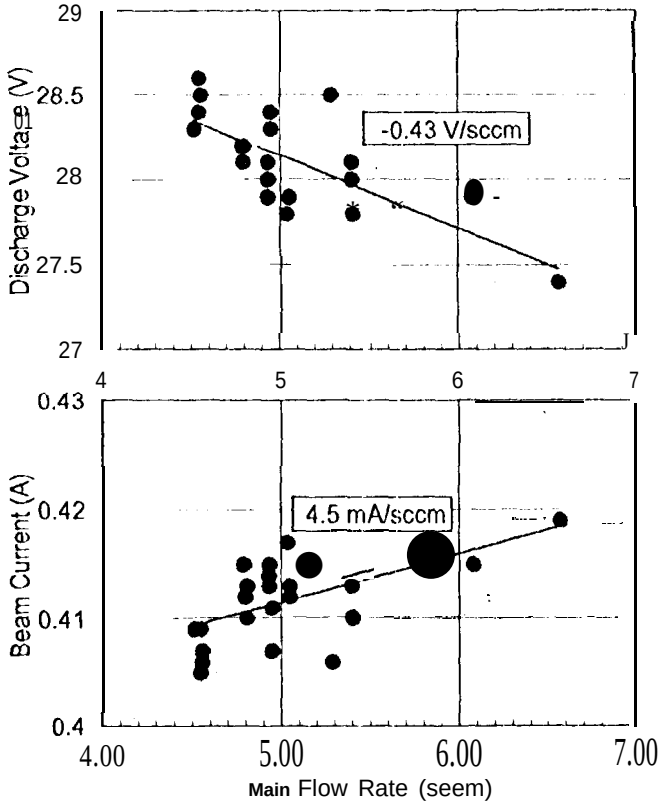

Fig. 9 Effect of large main flow rate changes (screen, accelerator, and decelerator grid voltages of 1320, -101, and -75 V, respectively, cathode flow rate of **1.32** seem).

hundred volts are unknown, if the sputter yield is comparable to that of graphite, then this carbon-carbon grid configuration operating with an accelerator grid voltage of- 100 V would have an extremely long life (with an erosion rate possibly more than 20 time-s less that corresponding to operation of a molybdenum grid at an applied voltage of -150 V).

The maximum beam current extracted to date from one segment with carbon-carbon grids was 700 mA. This was achieved with a screen voltage of 1450 V, an accelerator grid voltage of -102 V and a decelerator grid voltage of -75 V. This corresponds to operation at an R-ratio of 0.93. With all four segments operating with a beam current of 700 mA, the segmented engine could produce a beam current of 2.8 A at a R-ratio of 0.93. Reducing the thickness of the accelerator and decelerator grids will reduce the ability to operate at high R-ratios, however, operation with R-ratios as high as 0.93 was demonstrated for a beam current of 650 mA with SAND optics and thin (500 pm) thick accelerator and decelerator grids with graphite electrodes.[5]

Multiple Segment Operation

In spite of the problems associated with the operation of the graphite grid set on segment D, the full segmented ion engine was operated with beam extraction from all four segments as indicated in Fig. 11. Beam neutralization for all four ion beams was accomplished from the single, centrally located neutralize cathode without difficulty. The operating point of each segment could be controlled independently of the other segments (with the exception of the high voltage *settings) and there* appeared to be no interactions between the segments other than the expected thermal effects.

The temperature at the rear of the discharge chamber of one segment operating alone at a beam current of 450 mA is 260°C while that of the adjacent non-operating segments was 110 "C. Operation of multiple

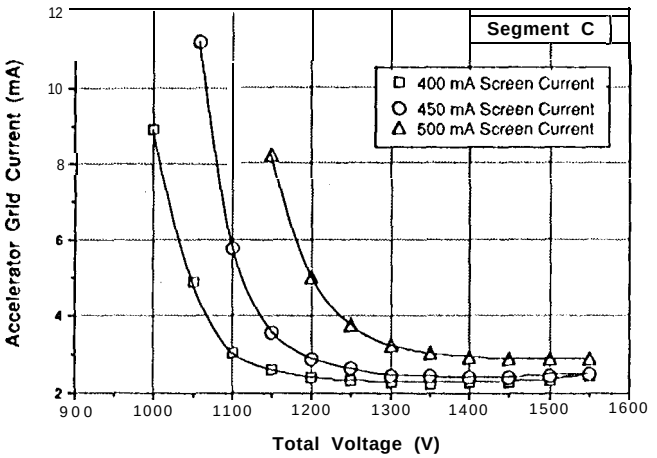

Fig. 10 Carbon-carbon grid perveance data for segment C.

segments at 450 mA beam currents each did not significantly increase the discharge chamber temperatures

Difficulties with the graphite grid set required that it be shut down and operation continued with the three segments equipped with carbon-carbon grids. Operation with segment combinations of A+B, B+C, A+C, and A+B+C was demonstrated, Discharge chamber performance curves for one segment could be obtained without affecting the operation of the other segments.

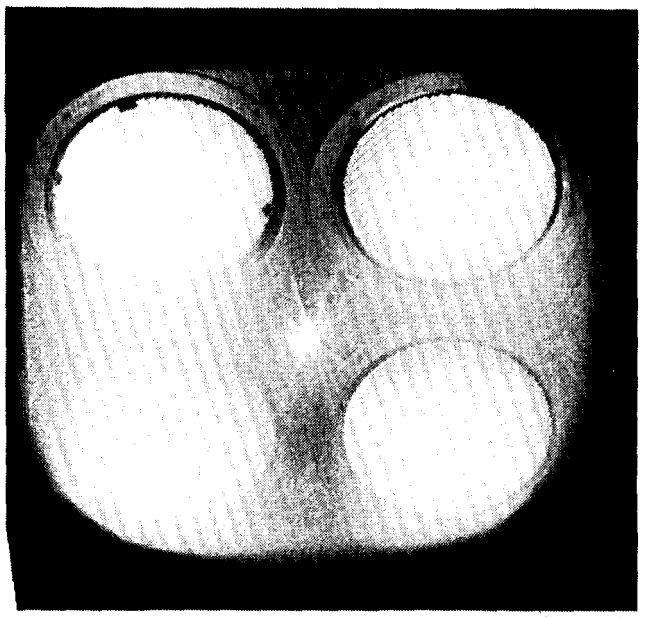

Fig. 11 Segmented ion engine with beam extraction from all four ion sources.

Beam Profile: To determine the beam divergence angle for the carbon-carbon grids and to search for evidence of beam interaction effects a the-axis positioning system was used to probe the ion beam current density profiles using a rake of Faraday probes. An example of the results of the beam scans are given in Fig. 12 for one and two segments operating. No adverse effects of multiple segment operation were observed. The preliminary beam current density data obtained to date suggests that the beam profiles do not appear to be additive so that the beam current densities measured for the segments operating alone do not add together to get the beam profile expected for multiple segment operation. The reasons for this are not clear and it is quite possible that this the result of a systematic measurement error rather than a real effect. A more complete description of the beam scanning results is given in Ref. 9.

Projected Performance: A maximum input power to the segmented engine of 2,4 kW was demonstrated with beam extraction from all four segments. However, operation of a single segment at up to 1,15 kW was also demonstrated with a beam current of 700 mA. With four segments operating at 700 mA each, the segmented ion engine is potentially capable of producing a beam current of 2,8A, with an input power of 4.7 kW, and producing a thrust of 170 mN with a specific impulse of 3700 s. Further work will be performed to expand the demonstrated operating range of the segmented thruster.

The performance data shown in Fig, 13 as the circular data points were obtained with segments A and C operating simultaneously at approximately constant beam currents of 500 mA each, The solid lines in this figure represent the performance projections from Ref. 4 for operation at a fixed beam current of 500 mA per segment. The specific impulse (and corresponding overall engine efficiencies) for the actual data points are less than that from Ref. 4 primarily because a high neutralizer cathode flow rate was used in the collection of the segmented thruster data, No attempt has yet been made to minimize the neutralizer nOw rate for the segmented thruster,

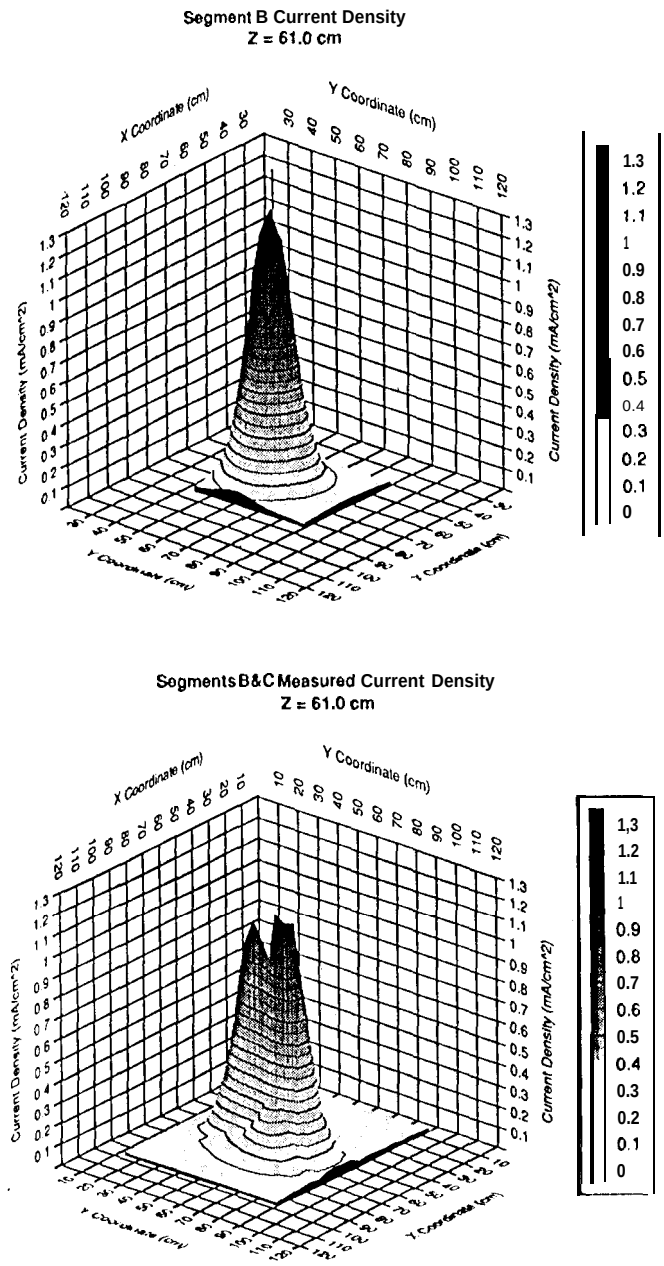

Fig. 12 **Beam** current density profile for segment **B** (top) and for simultaneous operation of segments **B** + C (bottom)

The performance goals for the segmented thruster are given in Fig. 14. These throttling curves were generated with the objective of maintaining the engine efficiency as high as possible over the throttling **range.** **This** **necessarily** implies operation at the maximum specific impulse, **Achieving** these goals **will** require improvement

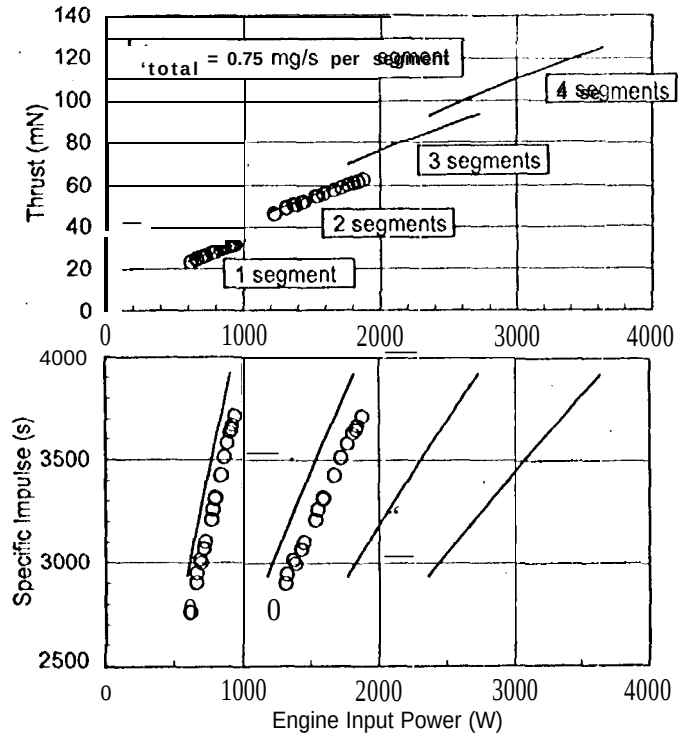

Fig. 13 Comparison of measured and projected thruser performance for throttling each segment at a constant beam current of **500** mA.

in the **perveance** of the carbon-carbon **grids** and a reduction in the **neutralizer** cathode flow rate. These data assume a constant accelerator grid voltage of -100 V which should be possible even for thin **accelerator** and decelerator grids **through** **the** **use** Of SAND **optics.** **The** **beam** **current** **in** **this** figure varied from a minimum of 300 **mA** to a maximum of 800 **mA** **per** segment.

The screen voltage, however, varied by only about 250 V, from 945 to 1200 V. The relatively small swing in screen grid **voltage** should simplify the **design** of this supply. The curves in Fig, 14 cover, an input power throttling range of 12 to 1 (from **0.38** **kW** to 4.64 **kW).**

Assuming the sputter yield of carbon-carbon is the same as graphite, and an accelerator grid voltage of -100 V, the grid life should be tens of thousands of hours at the maximum power point. The **projected** time required **to** **achieve** a **specified** total throughput for the engine is given in Table 2 as a function of the beam current per segment. At a beam current of 700 **mA** **per** segment (2.8 A total) a propellant throughput capability of 120 kg could be **demonstrated** in approximately 8000 hours. A thorough understanding of the **engine** failure mechanism through the application of probabilistic physics of failure techniques

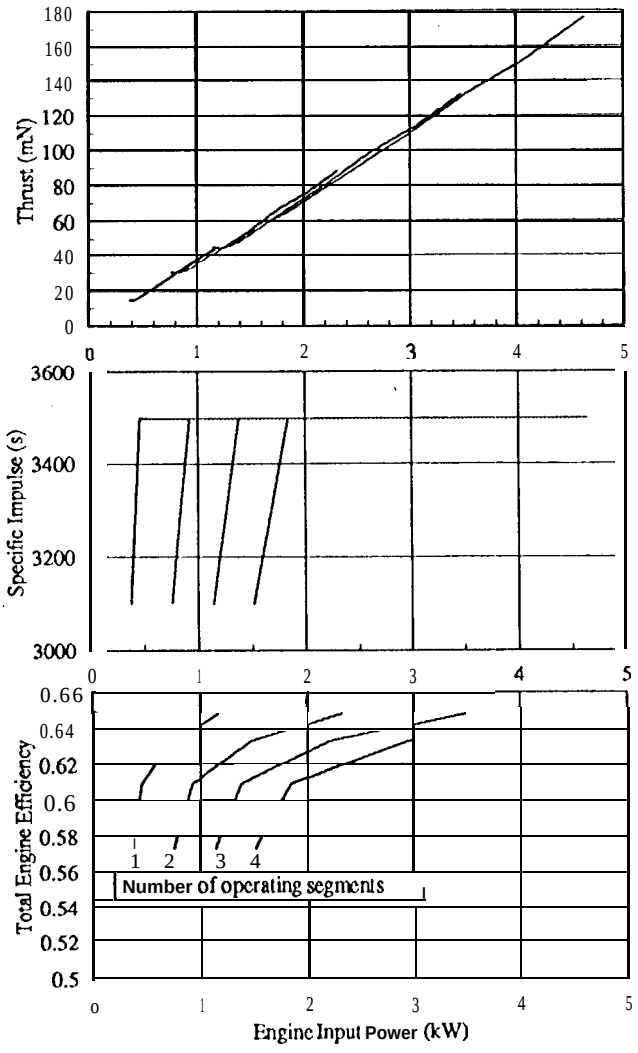

Fig. *14* Performance objectives for the segmented ion engine with maximum efficiency throttling.

will be required to credibly establish the service life or throughput capability of the engine.

Projected System Masses

Component masses for the propulsion system based on the use of a single 4x15-cm segmented ion engine and a single, internally-redundant power processor unit (PPU) arc given in Table 3. For the projected performance given in Fig. 14 and reasonable projections of PPU efficiency, this system would be capable of operating over an input power variation from 300 W to 5 kW. The total projected dry mass for the system is approximately 98 kg (not including the solar array or power management and distribution hardware which is assumed to be included in the host spacecraft). For a propellant loading of approximately 100 kg we see that the propulsion system dry mass is still approximately 50 % of the wet mass, but the specific mass is only 20 kg/kW (for a maximum input power of 5 kW).

The major difficulty with this approach appears to be that the gimbal mechanism becomes a single point failure for the mission. The engine is a single point failure only in the beginning of the mission when it is operating a full power. For throttled conditions one or more segments may be turned off and may therefore be considered to be redundant components, Electrical isolation of the segments allows a fault in one segment to be isolated from the others. For spacecraft designed such that the maximum power available to the propulsion system is less than 3.8 kW, then the segmented engine would never be operated with more than three segments on at a time, so that the fourth segment could be considered a spare.

Conclusions

A light-weight, compact segmented ion engine consisting of four 15-cm diameter ion sources was successfull y fabricated and tested over a power range from 600 to 2400 W, Operation with beam extraction from one, two, three and four ion sources was demonstrated with beam neutralization being provided by a single neutralizer cathodc. Ion accceleration from all four ion sources was accomplished from a single high voltage screen supply, Operation of a single 15-cm ion source at up to 1.15 kW with a beam current of 700 mA was also demonstrated, suggesting an input power capability with all four segments operating of 4.6 kW. Successful operation of flat carbon-carbon grids in a three-grid SAND configuration was demonstrated on the three ion sources equipped the carbon-carbon grids. Operation at net-to-total voltages of 0.93 at beam current in one ion source of 700 mA (equivalent to 2.8 A for the full segmented engine) holds the promise of very long useful grid lifetimes and high total throughput capabilities, A 5-kW propulsion system based on the use of a single 4x15-cm segmented ion engine has a projected mass of approximately 100 kg for a conservative propellant loading of 100 kg of xenon. Further work will foeus on expanding thc demonstrated operating envelope of the segmented engine with carbon-carbon grids and assessing the service life (and throughput) capability of the engine,

Acknowledgments

The authors thank Mr. Alison Owens, Mr. William Thogmartin and Mr. Robert Toomath for assembling the segmented ion engine and support hardware. The work described in this paper was performed by the Jet Propulsion Laboratory, California Institute of Technology, under contract with the National Aeronautics and Space Administration.

References

[1]Sauer, C. G. and Yen, C. L., "Planetary Mission Capability of Small Low Power Solar Electric Propulsion Systems," IAA-L-0706, presented at the IAA International Conference on Low-Cost Planetary Missions, Laurel, Maryland, April, 1994.

[2]Kakuda, R., Sercel, J., and Lee, W., "Small Body Rendezvous Mission Using Solar Electric Ion Propulsion: Low Cost Mission Approach and Technology Requirements," IAA-L-O71O, presented at the IAA International Conference on Low-Cost Planetary Missions, Laurel, Maryland, April 1994.

[3]Nagano, H., Gotoh, Y., and Nishida, E., 'Development of Ion Engine System for ETS-VI," ISTS-94-a-63, presented at the 19th International Symposium on Space Science and Technology, Yokohama, Japan, May, 1994.

[4]Brophy, J. R., "A Segmented Ion Engine Design for Solar Electric Propulsion Systems," *Space Technol.* Vol. 14, No. 1, pp. 73-80, 1994, Pergamon.

[5]Brophy, J. R., Pless, L. C., Mueller, J., and Anderson, J. R., "Operating Characteristics of a 15-cm-dia. Ion Engine for Small Planetary Spacecraft," IEPC-93-110, presented at the 23rd International Electric Propulsion Conference, Seattle, WA, September, 1993.

[6]Brophy, J. R., Pless, L. C., and Garner, C. E., "Ion Engine Endurance Testing at High Background Pressures," AIAA-92-3205, presented at the 28th Joint Propulsion Conference, Nashville, TN, July, 1992.

[7]Patterson, M. J., Haag, T. W., "Performance of the NASA 30-cm Ion Thruster," IEPC-93-108, presented at the 23rd international Electric Propulsion Conference, Seattle, WA, 1993.

'Mueller, J., Brophy, J. R., Brown, D. K., and Garner, C. E., "performance Characteristics of IS-cm Carbon-Carbon Composite Grids," AMA-94-31 18, to be presented at the 30th Joint Propulsion Conference, Indianapolis, IN, June, 1994.

[9]Tierney, M., Brophy, J. R., Mueller, J., "Segmented Ion Engine Plume Characteristics," AIAA Paper No. 94-2740, to bc presented at the 30th Joint Propulsion Conference, Indianapolis, IN, June, 1994.

[10]Beattie, J. R., Williams, J. D., and Robson, R. R., "Flight Qualification of an 18-mN Xenon Ion Thruster," AIAA-93-1085, presented at the AIAA/AHS/ASEE Aerospace Design Conference, Irvine, CA, February, 1993.

[11]Krauthamer, S. and Das. R., Interoffice Memorandum, "Converter System Job #9447JC1207000," August 27, 1992, JPL internal document.

[12]Stevens, D. M., Interoffice Memorandum, "Discussion on Xenon Feed Systems," April 7, 1994, JPL internal document.

[13]Personal communication, Juergen Mueller, Member of the Technical Staff, Jet Propulsion Laboratory, California Institute of Technology, May 1994.

[14]Miyake, R. N., Interoffice, "Thermal Evaluation of Propulsion S ystem Power Processing Unit (PPU)," May 25, 1994, JPL internal document.

Table 1 Grid Geometries

Parameter	Carbon-Carbon Grid Set 1 (Segment A)	Carbon-Carbon Grid Set 2 (Segment B)	Carbon-Carbon Grid Set 3 (Segment C)	Graphite Grid Set (Segment D)
Screen Grid				
Thickness (mm)	0.52	0.44	0.56	0.46
Hole Dia. (mm)	1.86	1.84	1.93	1.78
Open Area Frac.	0.64	0.63	0.69	0.59
Gap (mm)	0.64	0.64	0.64	0.76
Accelerator Grid				
Thickness (mm)	0.94	0.93	0.94	0.51
Hole Dia. (mm)	1.18	1.18	1,15	1.14
Open Area Frac.	0.26	0.26	0.25	0.24
Decelerator Grid				
Thickness (mm)	0.94	0.94	0.94	0.51
Hole Dia. (mm)	1.70	1.78	1,72	1.60
Open Area Frac.	0.54	0.59	0.55	0.47
Gap (mm)	0.25	0.38	0.25	0.76

Table 2 Time Required for Total Propellant Throughput

Beam current per Segment (mA)	Total Beam Current (A)	80 kg of Xenon	100 kg of Xenon	120 kg of Xenon
500	2.0	7480 hrs	9350 hrs	11220 hrs
600	2.4	6230 hrs	7790 hrs	9345 hrs
700	2.8	5340 hrs	6675 hrs	8010 hrs
800	3.2	4670 hrs	5840 hrs	7005 hrs

Table 3 5 kW System Mass Estimate

item	unit Mass (kg)	QTY	Contingency (%)	Total Mass (kg)	Reference
4x15-cm segmented Engine	8	1	10	8.8	Mass of lab model thruster
PPU	31.3	1	15	36.0	From Ref. 11 with rough approximation for internal redundancy
Gimbal	4.0	1	30	5.2	Ref. 2
Tank	3.9	1	30	5.1	Ref. 12 for 100 kg of Xe
Feed System	9.6	1	10	12.5	Ref. 12
DCIU*	0.5	1	30	0.7	Ref. 13
PPU Thermal	6	1	30	7.8	Ref. 14
Non-PPU Thermal	3.4	1	Included	3.4	5 % rule of thumb (Ref. 2)
Cabling	3.4	1	Included	3,4	5 % rule of thumb (Ref. 2)
structure	12.1	1	Included	12.1	6.5% of wet mass (Ref. 2)
Valve Drive Unit	2	1	30	2.6	ETS-VI (Ref. 3)
Total Dry Mass (without Contingency)	***84.2***		***Total Dry Mass (with Contingency)***	***97.6***	

**Digital* Interface and Control Unit (assumed to be physically integrated into the PPU)